Docket No. SA-522

Exhibit No. 2-X

NATIONAL TRANSPORTATION SAFETY BOARD

Washington, D.C.

AIAA 2002-4715, An Engineering Study of the Unsteady Response of a Jet Transport During a Wake Encounter in a Transitional State of Potential Crow Instability, AIAA Atmospheric Flight Mechanics Conference

(12 Pages)

AIAA 2002-4715

An Engineering Study of the Unsteady Response of a Jet Transport during a Wake Encounter in a Transitional State of Potential Crow Instability

A P Brown
National Research Council
Ottawa, Canada

AIAA Atmospheric Flight Mechanics Conference
5-8 August 2002
Monterey, California

(2)

An engineering study of the unsteady response of a jet transport during a wake encounter in a transitional state of potential Crow instability

A P Brown

National Research Council
Ottawa, Canada

ABSTRACT

An engineering study has been conducted into the unsteady motion and loads response of a widebody jet transport encountering a vortex wake from a preceding 'heavy' aircraft, the wake undergoing a transitional change of flow-state from a trailing-pair through a Crow instability mechanism to a train of vortex rings. It is postulated that, having formed, the migratory Crow instability vortex rings have then rotated to the more stable upright position (coaxial with the downwash vector). The second aircraft is assumed to follow a flight path through the vortex cores of the right side of the vortex rings at 260 knots. On this flight path the estimated strength of the vortex rings is such that the induced velocity produces sideslip angle excursions to ±10°, with extremely dynamic reversals, *up to 200°/sec. Accounting for sideslip, lateral and yaw* accelerations, the fin loads have been estimated using indicial functions. A yaw damper operating on a simple rate law is calculated to slightly reduce the responsive motion, *albeit* with a mild increase in fin loads. If reactive pilot rudder inputs are assumed, the analysis indicates that, depending upon sensory/system input-output lag, it could be possible to couple the rudder activity in-phase to each subsequent vortex ring encounter in which case, significant magnification of fin loads is estimated to occur, of the order of 30-35% greater than that estimated without reactive, dynamic rudder input commands. For the subject transport aircraft, this would represent peak load values of the order of twice the estimated critical design manoeuvre limit load case.

NOMENCLATURE

a	vortex ring radius, m
A	sectional area, m^2
b	wingspan (wake-generating aircraft of following aircraft, as applicable), m
$\bar{c}$	mean aerodynamic chord, m
c	wave transmission speed, m/s
C_{Yj}	derivative coefficient of aerodynamic sideforce with respect to kinematic quantity j, $C_{Yj}=\partial(Y/½\rho U^2 S)/\partial j$
C_{nj}	derivative coefficient of aerodynamic yawing moment with respect to kinematic quantity j, $C_{nj}=\partial(N/½\rho U^2 Sb)/\partial j$
E	Young's modulus, N/m^2
E	elliptic integral of the second kind
f	frequency, s^{-1}
i	pertaining to the *i*th vortex ring
I_y	sectional moment of area, m^4
I_{ZZ}	polar moment of inertia, about aeroplane normal axis, passing through the centre of gravity, kgm^2
K	elliptic integral of the first kind
K_W	*Wagner function*
l_p	length from the CG to the FLT.STA, following aircraft, m
l_v	length from the aerodynamic centre of the fin/rudder (AC_V) to the FLT.STA, m
L	length, m
m	aeroplane mass, kg
m_i	elliptic integral parameter
N	aerodynamic yawing moment
r	yaw rate, rad/sec
s	non-dimensional time, $Ut/\bar{c}$
S	wing area, m^2
t	time, sec
U	freestream air velocity, m/s
V	induced velocity components, m/s
x_i	axial distance (*i.e.* along flight path and normal to the vortex ring plane) from the plane of the *i*th vortex ring, m
y	aeroplane lateral displacement, m
Y	aerodynamic sideforce
z	aeroplane normal axis direction
β	sideslip angle, deg
Δx	vortex ring separation, m
Δx	small axial distance increment, used in the numerical formulation of V_σ, m
Γ	vortex strength, m^2/s
φ	yaw angle, deg
μ	inertial parameter, $2m/\rho S\bar{c}$
μ_I	inertial parameter, $2I_{ZZ}/\rho bS\bar{c}$
ρ	air density, kg/m^3
ρ	structural material density, kg/m^3
σ	radial distance from the vortex ring axis (in cylindrical co-ordinates), $\sigma_1=\sigma_2=\sigma_3$, *m*
ζ	rudder deflection, deg
ψ(x,σ)	stream function
ψ	yaw angle, rad

subscripts:

i	*i*th vortex ring
r	rudder
t	time
v	fin/rudder location
x	axial direction
σ	radial direction

BACKGROUND

Contemporary takeoff and landing separation standards for civil transport aircraft (for example, those of Ref.1) have been established by considerations of the strength and migratory trajectories (against the influence of the earth ground-plane) of the trailing vortices of preceding transport aircraft wakes. Separation standards have been established by consideration of the dissipative and migratory vortex wake characteristics in conjunction with influential variables, which include wind strength, wind direction, atmospheric profile, atmospheric turbulence and the preceding aircraft parameters of Type Design, mass, airspeed and configuration.

In establishing separation standards, the vortex interaction of concern is a 'near-coaxial' encounter between

3

the vortex wake (developed as a highly-discretised – in terms of vortex-scale – trailing pair of line vortices) and a following aircraft with a nearly-parallel flight path. As such, the aerodynamic effect of the interaction is principally a roll upset, which potentially could become a roll/yaw departure from controlled flight, due to the relatively low-speed (and high angle-of-attack) of the following aircraft. Hence, the fluid dynamic research emphasis for the determination of separation standards has been based upon wake lengths of 1 to 6 miles, relative to the ground, and age ½ to 3 minutes.

Rossow and James[2] present the results of an observational study into interactions between following aircraft and preceding aircraft wakes, with an emphasis upon the cruise condition of flight. In cruise encounters, compared to takeoff/landing approach, three other additional parameters are significant – high speed, across-trail encounter angle and wake age. Cruise interactions involve much greater longitudinal separation (by an order of magnitude) and hence wake age than that used for establishing takeoff and landing separation standards.

In some contemporary ATC radar environments, jet transports are typically climbing at airspeeds of 250 knots IAS within two minutes of lift-off and upon descent, are often permitted to maintain high airspeeds within the range of 250 to 340 knots IAS until initial approach or base-turn altitudes of a few thousand feet. With this in mind, the cruise wake considerations of Ref. 2 can be extended to 4th segment (enroute) takeoff climb and descent/initial approach flight phases.

In terms of the magnitude of unsteady aerodynamic loading during such encounters, wake age may be a fundamentally determining parameter. In the consideration of takeoff and landing separation standards[1], the preceding aircraft wake is generally in the rolled-up vortex sheet state (*i.e.* a pair of stable counter-rotating trailing line vortices). The takeoff or landing stable vortex pair state can last for several minutes, depending upon the spanwise distribution of bound-circulation and the distribution/characteristics of shed vorticity. However, for cruise altitude, speed and circulation conditions, Ref.2 defines the observed ageing-wake states as:

	State:	*Time:*
(1)	Vortex sheet roll-up	0-10 sec
(2)	Instability development & wake division	0-2 min
(3)	Vortex loop subsidence, wake reformation	2-5 min
(4)	Wake re-organisation to a vortex pair	5-15 min
(5)	Development of condensation striations	15 min-1 hr
(6)	Loss of condensation trial identity	>1 hr

The first three states are depicted in Figure 1.

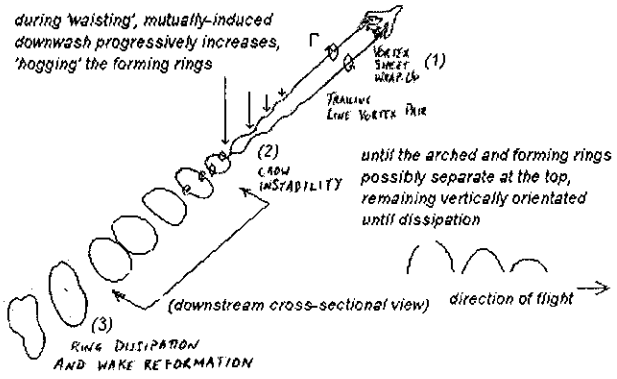

Figure 1 – Pictorial description of Crow instability process in a vortex wake consisting initially of a developed pair of trailing line vortices (not to scale), refs. 1, 2 and the author's observations.

States 2 and 3 are states of vortex transition and/or breakdown. Of significance in the above list is the lack of a stable vortex-pair state following roll-up, unlike takeoff or landing approach. It is probable that lesser circulation in cruise, compared to takeoff or landing approach, is an important reason for the difference. Therefore, it is possible that during climb-out transition to high speed, and during descent transition from high speed, the types of wake-state may transition from stable vortex-pair types to early-instability types, and *vice versa*, respectively.

Hence, upon climb-out or initial approach, a following aircraft at two minute takeoff separation could encounter a preceding wake which is not in a stable vortex-pair state, but rather which is in a state of breakdown or transition. Concerning State 2 instability modes: one such mode is the long-wave or Crow instability[3], wherein the tip/rolled-up sheet vortex pair divides into a broken chain of vortex rings. It is reasoned that this process would result in temporarily and locally higher induced velocity magnitudes and would increase the vortex-crossing angle for a following aircraft on a coaxial flight path; in comparison, other State 2 instability mechanisms are short-period and involve the re-distribution of vorticity from discrete large-scale eddy cores to distributed scales of turbulent eddy sizes, mechanisms which could involve the production ('bursts' of localised higher velocities) and dissipation of turbulent energy.

Encounters, coaxial or otherwise, with such wake states might give rise to transient aerodynamic loads of magnitudes beyond that induced by stable trailing vortex states – which have been analysed and measured in detail. In comparison, an understanding of the fluid mechanics of wake states 2 and 3 arguably suffers from a lack of full-scale flight data. In the view of Rossow and James[2], studies of the fluid dynamics of cruise wakes by inflight probing are warranted.

In the present paper, considerations are limited to Crow instability State 2 wakes. In particular, an engineering study has been conducted of the response of a following widebody jet transport during a Crow instability wake encounter, wherein the vortex rings are assumed to have rotated to the downwash-normal direction.

CROW INSTABILITY WAKE

The process of long-wave or Crow instability is illustrated in Figure 1. In cruise vortex wakes visualised by condensation, the instability appears to consist of a mutual attraction between trailing vortices, resulting in spatially-periodic migration of the line vortices together or 'waisting', arching or 'hogging' (Fig. 1) due to the increased mutually-induced downwards velocity, and finally pinching and linking to become a series of curved vortex segments or possibly rings, perhaps inclined more-or-less vertically. Thereafter, the vortex elements dissipate in a wake reformation process. The ring formation and dissipation/wake reformation process might occur quickly (*e.g.*, for the Hawker Sea Fury aircraft, the vortex rings have been observed by the author to occur in a wake age of about five seconds and last for about fifteen seconds). On the other hand, depending upon vortex scale-size and characteristics, notably the core and core-edge vorticity distribution, they may last for a significant time.

Condensation trail observations of cruising jet transports indicate relatively long Crow instability durations of about ½ to 1 minute. The author's inflight observations of Crow instability vortex elements indicate that following the waisting and hogging process, the loops then appear to separate at the bottom of inverted 'U' shapes, forming upright arched vortex rings, which may possibly then separate at the top to form smaller rings. It is conjectured that, before dissipation and wake reformation occurs, the waisting and separating process

could result in upright vortex ring elements which are upright (as hypothesised in Figure 1) and coaxially aligned with the downwash flow of the wake before further breakdown. For analytical simplification in this directional interaction study, a vortex flow-state consisting of quasi-steady vertical rings has been chosen for the study.

As shown in Figure 2, a following aircraft, outside or near the lateral edges of vortex rings, would encounter lateral-direction induced velocities – for an aircraft on the equatorial line of the ring the encounter would consist of a series of reversing directional perturbations, due to unsteady fin/rudder sideforces, the development of which will at least partly shear the vortex. The interaction between the sheared vortex and fin/rudder may lead to increased circulation and aerodynamic forces produced at the fin/rudder.

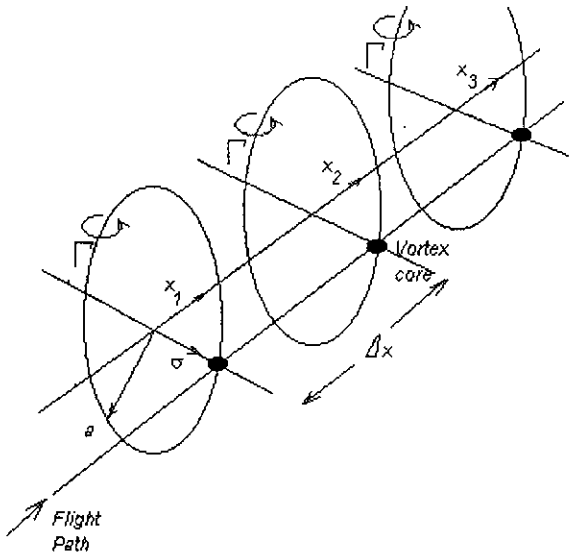

Figure 2 – Idealised train of vortex rings, vertically inclined with axes parallel and collinear, as assumed in the present study

VORTEX RING INDUCED VELOCITY MODEL

For the present engineering study, an encounter with three vortex rings is assumed. The vortex ring axes are assumed to be coincident. The aircraft undergoing the encounter is assumed to be flying parallel to the vortex ring system axis, along an equatorial flight path through the vortex cores, as shown in Figure 2.

For such a model, due to the highly spatially-discretised nature of the vorticity distribution, potential flow theory is presumed to provide a reasonable approximation. Certainly this has been an accurate representation for numerous studies of the trailing vortex pair, prior to the development of instabilities (for example, the work of Mather[4] and Treddenick[5]). Also supporting this assertion indirectly, the author[6] has analysed a thermally-driven free vortex inflight encounter, from MacPherson and Betts[7], and demonstrated that a potential flow line vortex model represented the mean flow structure accurately on that occasion. Furthermore, the analysis[6] indicated that *RMS* turbulent velocity levels of 10 to 15% of mean induced velocity magnitude existed at the axisymmetric edge of the vortex core. For the present study, no core-edge turbulence has been assumed, a non-conservative simplification from the viewpoint of unsteady loads analysis.

From potential-flow theory, the axisymmetric flow stream function for each vortex ring is given, for example Batchelor[8], as:

$$\psi_i(x_i,\sigma_i)=\Gamma\frac{(a\sigma_i)^{1/2}}{2\pi}\left\{\left(\frac{2}{m_i}-m_i\right)K(m_i)-\frac{2}{m_i}E(m_i)\right\}$$

with

$$m_i^2=\frac{4a\sigma_i}{\{x_i^2+(\sigma_i+a)^2\}}$$

K and E are the elliptic integrals of the first and second kinds respectively, Γ is vortex ring strength and (x_i,σ_i) is the axis system for each vortex, in cylindrical polar coordinates; as the vortex rings are coaxial, $\sigma_1=\sigma_2=\sigma_3=\sigma$. Superposition can be applied, such that the stream function for the total induced velocity due to the three vortex rings becomes:

$$\psi(x,\sigma)=\sum_{i=1}^{3}\psi_i(x_i,\sigma_i)$$

Thence, the x (axial) and σ (radial) direction resultant velocity components are given by[8]

$$V_x=\frac{1}{\sigma}\frac{\partial\psi}{\partial\sigma}$$

and

$$V_\sigma=-\frac{1}{\sigma}\frac{\partial\psi}{\partial x}$$

From these relations, the flowfield velocities along the flight path have been determined by numerical analysis, using forward differencing:

$$V_x=\frac{1}{\sigma}\frac{\psi_{\sigma+\Delta\sigma}-\psi_\sigma}{\Delta\sigma}$$

and

$$V_\sigma=-\frac{1}{\sigma}\frac{\psi_{x+\Delta x}-\psi_x}{\Delta x}$$

In accordance with the Biot-Savart law, vortex strength is conserved, so that $\Gamma_1=\Gamma_2=\Gamma_3=\Gamma$ and is estimated from $\Gamma=(L/b_{eff})/\rho V$ for the wake-generating aircraft, which is taken to be a large transport flying of wingspan b=79.8 m, flying at 250 KCAS with an assumed effective span loading of 69,646 N/m, giving $\Gamma=511 m^2/s$ at 3,000ft/ISA.

DIRECTIONAL EQUATION OF MOTION SOLUTION

For simplification of the present engineering study, the lateral-directional equations of motion have been decoupled. Given the highly dynamic nature of the encounters, the event duration of which is decoupled from the significantly longer period of lateral/directional modes, notably dutch roll (time comparisons being about one second and roughly five seconds, respectively), this is an acceptable simplification. Thence,

$$\begin{bmatrix} m \\ I_{zz} \end{bmatrix}\begin{bmatrix} \ddot{y} \\ \ddot{\varphi} \end{bmatrix}=\begin{bmatrix} Y \\ N \end{bmatrix}$$

with

$$\begin{bmatrix} Y \\ N \end{bmatrix} = \begin{bmatrix} Y_{\beta_r} & Y_r & Y_\varsigma \\ N_{\beta_r} & N_r & N_\varsigma \end{bmatrix} \begin{bmatrix} \beta_r \\ r \\ \varsigma \end{bmatrix}$$

as the unsteady aerodynamic forcing functions, in which: β_r is the resultant sideslip angle which is the sum of the externally-induced sideslip β, the yaw angle ψ from the t=0 undisturbed position and the lateral velocity $\partial y/\partial t$, again from the undisturbed position (using the standard aircraft displacement sign convention):

$$\beta_r = \beta + \frac{1}{U}\frac{\partial y}{\partial t} - \psi$$

Although included in the formulation for β, changes in longitudinal airspeed due to V_x are neglected in the above equation of motion formulation and in the derivation of the progressive build-up in aerodynamic force/moment magnitudes – based upon order of magnitude considerations, an acceptable simplification for the study.

For the unsteady growth of aerodynamic force and moment, indicial functions are used. Neglecting V_x as discussed above, all growth effects are a result of 'directional' angle changes (from an aerodynamic viewpoint, changes in fuselage and vertical surface incidence – the resultant angle of sideslip β_r ; any momentary super-circulation effect associated with the convection of the locally sheared vortex rings are not included in the model), for which the Wagner function K_W is an applicable indicial function, so that at time t:

$$I\ddot{\psi} = \frac{1}{2}\rho U^2 Sb \left\{ \begin{array}{l} C_{n_\beta} \int K_W(t-t')\dot{\beta}_r dt' \\ + C_{n_\varsigma} \int K_W(t-t')\dot{\varsigma} dt' \\ + C_{n_r} \int K_W(t-t')\ddot{\varphi} dt' \end{array} \right\}$$

and

$$m\ddot{y} = \frac{1}{2}\rho U^2 S \left\{ \begin{array}{l} C_{Y_\beta} \int K_W(t-t')\dot{\beta}_r dt' \\ + C_{Y_\varsigma} \int K_W(t-t')\dot{\varsigma} dt' \end{array} \right\}$$

With non-dimensional time as

$$s = Ut/\bar{c}$$

the equations reduce to

$$\ddot{\psi} = \left(\frac{U}{\bar{c}}\right)^2 \frac{\bar{c}}{\mu_I} \left\{ \begin{array}{l} C_{n_\beta} \int K_W(s-s')\frac{\partial \beta}{\partial s} ds' \\ + C_{n_\varsigma} \int K_W(s-s')\frac{\partial \varsigma}{\partial s} ds' \\ + C_{n_r} \int K_W(s-s')\frac{\partial^2 \varphi}{\partial s^2} ds' \end{array} \right\}$$

and

$$\ddot{y} = \left(\frac{U}{\bar{c}}\right)^2 \frac{\bar{c}}{\mu} \left\{ \begin{array}{l} C_{Y_\beta} \int K_W(s-s')\frac{\partial \beta_r}{\partial s'} ds' \\ + C_{Y_\varsigma} \int K_W(s-s')\frac{\partial \varsigma}{\partial s'} ds' \end{array} \right\}$$

wherein the inertial group parameters are

$$\mu_I = 2I_{ZZ} / \rho S b \bar{c}$$

and

$$\mu = 2m / \rho S \bar{c}$$

The Wagner function numerical expression for small aspect ratio, from R. T. Jones[9], as recounted by Fung[10], and as typically applied in design (see Lomax[11]) has been used in the present study.

The $[Y\ N]^T$ pair of equations are interdependent. They have been solved for induced sideslip $\beta(t)$ as the *a priori* aerodynamic forcing function waveform, using an iterative time-marching algorithm. At time $t=t+\Delta t$ following each time-step, an initial $[Y\ N]^T$ solution loop establishes initial values for the responsive state vector:

$$[\partial^2\psi/\partial t^2\ \partial\psi/\partial t\ \psi\ \partial^2 y/\partial t^2\ \partial y/\partial t\ y]_t$$

Thereafter, an iterative-solution loop of the $[Y\ N]^T$ equation pair updates this vector. For cases (ii) and (iii) below, five iterations provide a fully-converged solution at time t.

Three cases have been included in the study:

(i) zero rudder deflection, simulating yaw damper (YD) OFF;
(ii) rudder deflection, in accordance with the solution of a yaw damper model, included in the iterative loop (simulating YD ON); and
(iii) rudder deflection, in accordance with the superposition of:
- the YD model output rudder deflection, and
- a pilot-input rudder pedal deflection, in accordance with a behavioural model.

For cases (i) and (ii), the equations have been solved for rigid-body solutions. For case (iii), fuselage transverse bending flexibility dynamics have been accounted for, using a simplistic and approximate methodology, which is nevertheless suitable to the study.

Wake-encounter aircraft data

For the study, all inertial, geometric and aerodynamic input data for the aircraft undergoing the wake encounter has been chosen to be representative of a swept-wing widebody jet transport.

For the aircraft, the following inertial and geometric data was used as input:

Mass:	154898 kg
Wingspan, b:	44.85 m
Length:	54.1 m
l_v, length, AC_V-FLTSTA:	25.1 m
l_P, length, CG-FLTSTA:	20.3 m
Fin/rudder MAC:	4.57 m
Izz:	18.77×10^6 kgm^2

Likewise, the following aerodynamic derivatives were used for all cases, primarily drawn from an average of the jet transport derivative data presented in Nelson[12]:

$C_{Y\beta}$	-0.90
$C_{Y\beta v}$	-0.38
$C_{Y\varsigma}$	0.19
$C_{N\beta}$	0.15
$C_{N\beta v}$	0.19
$C_{N\varsigma}$	-0.10

6

Vortex ring train sizing

In the idealised model of the present engineering study, the dimensions of each vortex ring have been assumed to be identical. The selection of dimensions has been based upon the approximate sizing of cruise wake Crow instability vortex rings, as indicated by the present author's observations and by the photographic observations of Ref. 3. Based upon these limited observations, the study has conducted analyses for the hypothesised vortex ring spacings of $3a$ and $5a$, a being the vortex ring radius. Using the size parameters of Figure 2:

Vortex ring radius, a:	$2(b_{eff}/2) = 63.8$m
Vortex core radius, r_c:	$0.1(b_{eff}/2) = 3.2$m
Longitudinal separation, Δx:	$3a = 191.5$m (5a is also considered, see later)

for which b_{eff} is the effective span of the wake-generating aircraft, assumed to be 80% of the geometric span, b, and assumed to equate to the lateral separation of the trailing line vortices (see Figure 2).

Yaw damper model

The yaw damper model was chosen to be a simple yaw rate-feedback system, no long-period washout (which would not be responsive in this study, in any case) or yaw acceleration sensing (for 'feedforward' gust alleviation) with the following assumed system characteristics:

System gain: -1, defined as output rudder deflection rate to sensed yaw rate, *i.e.* $\partial\zeta/\partial t=-\partial\psi/\partial t$, up to a max. ζ actuation rate of 39 deg/sec, as limited by a YD rate limiter;

System/actuator lag: 6.25 milliseconds (ms)

Human-machine interface model – rudder deflection

The fin/rudder unsteady air loads accompanying the vortex ring encounters are very short duration events. In practice, it is likely that they would be preceded by some initial wake turbulence, to which the pilot response may well be to 'ride-through', without intervention – but which would conceivably 'key' the pilot towards an interventionary frame of mind. If a subsequent wake-induced perturbation was of an alarming magnitude and rapidity, in deciding to intervene the pilot response would conceivably be a rate-saturating reactive response rather than a proportional response.

Therefore, for modelling the highly dynamic environment, the human-machine-interface (HMI) rudder deflection model was chosen as a high gain reactive system, such that rudder deflection would be limited by the rudder deflection rate limiter, rather than by rudder pedal actuation rate. The following HMI system characteristics were used:

Controller: *reactive* human control, requiring an initial 'GO' decision, thereafter an ON-OFF-ON switch-reversal type of control: switching being based upon the perceived lateral acceleration reaction at the flight station (FLT.STA); assumed switch thresholds of:

ON: $\partial\zeta/\partial t=-[\partial\zeta/\partial t]_{S.M}\cdot\{(\partial^2y/\partial t^2)/|\partial^2y/\partial t^2|\}_{F/S}$ at a threshold of $\Delta|\partial^2y/\partial t^2|_{F/S}\geq 0.3$g

OFF-ON: a rudder reversal applied when the $(\partial^2y/\partial t^2)_{F/S}$ magnitude reverses through 0.1g in the other direction

System gain: High gain piloting, resulting in rate saturation, such that rudder pedal actuation rate exceeds rudder actuation rate, which is therefore limited to that of the assumed maximum rate limiter value of $[\partial\zeta/\partial t]_{S.M}=39$ deg/sec;

System lag: various lags have been studied over the range from 25 to 100 ms; although it is questionable whether this value is realistic for initial intervention (for which lags of 120-250ms might be more realistic), arguably such fast response times might very well be realistic for high gain reactive control reversal inputs after the initial intervention.

The choice of reactive human control and the compulsion to 'GO' (the reactive trigger) in the HMI decision-making process are discussed in the relevant results and discussion section.

Vertical stabiliser design manoeuvre loads

For jet transport aircraft, the design manoeuvre load cases are specified in FAR 25.351(a)[13] and JAR 25.351(a)[14].

The three cases represent:
(1) maximum ζ at zero sideslip;
(2) resultant β with maximum ζ; and
(3) zero ζ at resultant steady β.

For each case, the design load on the vertical stabiliser (fin/rudder combination) at any particular $[V\ \zeta]_{DESIGN}$ will be proportional to the sideforce coefficient, in general:

$$C_Y=C_{Y\beta}\beta+C_{Y\zeta}\zeta$$

so that for each of the three cases,

(1) $C_Y=C_{Y\zeta}\zeta_{MAX}$
(2) $C_Y=[C_{Y\zeta}-f_{DYN}(C_{n\zeta}/C_{n\beta})]\zeta_{MAX}$ (expressing the peak sideslip angle as a factor $f_{DYN}>1$ and noting that in steady state $\beta=-(C_{n\zeta}/C_{n\beta})\zeta_{MAX}$
(3) $C_Y=-C_{Y\beta V}(C_{n\zeta}/C_{n\beta})\zeta_{MAX}$

Of these, for the derivative values chosen for the aircraft of the present study, case (3) is critical. Accordingly, noting that for typical design c_f/c values of about 28% $C_{Y\beta V}=2\ C_{Y\zeta}$, the limit load at the datum flight condition is selected as:

$$P_{Vlim}=\tfrac{1}{2}\rho V^2S[-2C_{Y\zeta}(C_{n\zeta}/C_{n\beta})\zeta_{MAX}]$$

with $\zeta_{MAX}=10°$ and V=260 KCAS, for the present study.

Fuselage transverse bending flexibility

The equation of motion solution for the three cases have been conducted as rigid body analyses. However, in the case of the pilot-activated rudder deflection, the inputs would be highly dependent upon the lag introduced by fuselage flexibility, in this case to transverse bending.

A rigorous analysis of the dynamic response of the fuselage and wing, since for yaw acceleration under fin loads the wing is accelerated in response to fuselage flexibility also would require a numerical solution. This could be based upon discretisation of mass-stiffness properties along the length of the fuselage, with the wing mass and inertia lumped onto the fuselage (acceptable because of the very high transverse stiffness of the wing) and solution of the matrix of Lagrange equations.

As a simplification acceptable for the purposes of the present study, the global effects of fuselage transverse bending flexibility have been modelled. The global effects are a dynamic magnification of impulsive loads (*i.e.* overswings) and a load-lag, due to strain wave transmission. Conservatively, a dynamic magnification factor of 1 for all loads, has been chosen for the present study. The lag introduced by flexibility is modelled by the wave transmission solution of Hussey[15] – the wave transmission speed for transverse flexure is given by

$$c^2 = \omega \sqrt{\left(\frac{EI_y}{\rho A}\right)_{fuse\ell - loaded}}$$

and the associated vibratory modal frequencies are given by:

$$f = \frac{\pi}{8L^2}\sqrt{\left(\frac{EI_y}{\rho A}\right)_{fuse\ell-loaded}} \quad (9.067,25,47,81...)$$

The frequency equation is used to check the sensibility of modal frequencies, for the widebody aircraft used in the present study. For a loaded fuselage mass of 73,500 kg, and sectional $I_y/A=3.3m^2$, the so-calculated frequencies of 6.1, 16.9 and 31.7 Hz are sensible.

Typically, for engineering purposes, bending transmission can be described by the first two wave frequencies, for example Abramson[15]. For the present study, the fundamental, first and second harmonics have been chosen to be sufficient to contain the flexural strain energy, which is assumed to be transmitted in distributed percentages of:

[F 1^{st} 2^{nd}]=[57 29 14]

RESULTS AND DISCUSSION

The results for the three cases, using the models and solution methodology as described are presented herein, for each of the three cases, in turn. Case results and discussions are preceded by a discussion on the perturbing flowfield.

Time reference, t

For all solutions, the time origin t=0 equates to the encounter aircraft being a short distance (approximately one vortex ring radius) upstream of the plane of the first vortex ring at x_1.

Flowfield, vortex ring train-induced sideslip, β

For the selected flight path, traversing the vortex cores along the vortex ring equatorial line, the solution of the induced flow stream function equation and numerical differentiation of the stream function gives rise to the perturbing sideslip function as presented in Figure 3, for which sideslip angle is defined in the axis sign convention as:

$$\beta = \arctan\left[\frac{-V_\sigma}{(U - V_X)}\right]$$

with the flight direction as positive in the same sense as the cylindrical polar x-direction, the σ-direction being positive outwards (refer Fig. 2).

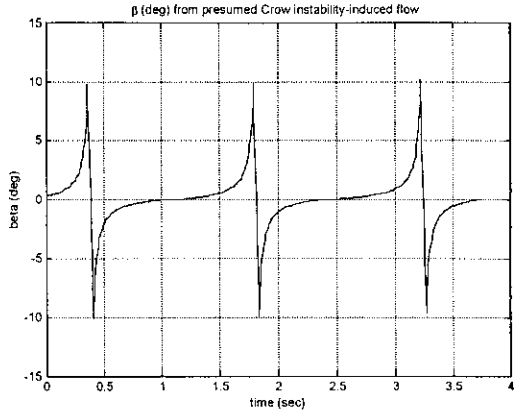

Figure 3 – Sideslip angle induced along a flight path in the axial direction, traversing each vortex core at the equatorial position, by the vortex ring train.

It is seen in Figure 3 that maximum perturbing sideslip values of ±10° would be encountered along such a flight line. As each vortex core is traversed, the sideslip rate change $\partial\beta/\partial t$ would be enormous, approximately ±200 deg/sec. During these periods, the development of aerodynamic force would be dominated by induced and convected local circulation due to the sheared vortex, for similar scale sizes between vortex core and fin/rudder mean aerodynamic chord (MAC).

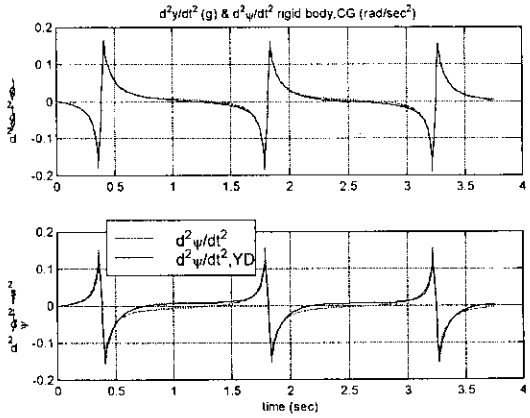

Figure 4 – CG Lateral acceleration and yaw acceleration, Case (i) and Case (ii)

Cases (i), zero rudder deflection, ζ, and (ii), yaw damper-driven rudder deflection (YD-ON)

The analyses for zero rudder deflection ζ, and for the yaw damper-driven rudder deflection case, have been undertaken as rigid body analyses, using the equations and solution methodology outlined previously.

In both cases, of particular interest are the output lateral and yaw accelerations, developed yaw rate, YD-driven rudder deflection and momentary fin loads, when compared to the most critical of design manoeuvre load cases.

The aircraft CG lateral and yaw accelerations for the two cases are shown in Figure 4, with reference to which it is

seen that YD-ON is mildly successful in ameliorating the effect of the impulsive lateral loading of each of the three sequential encounters with a vortex ring, insofar as the yaw acceleration following vortex-core passage subsides more quickly. As expected, without feedforward (*i.e.* such as yaw acceleration sensing or, most responsively lateral acceleration sensing at the location of the fin), YD-ON does not reduce the responsive yaw acceleration peak values, approximately 0.14 rad/sec^2. Although not apparent in Figure 4, the yaw acceleration values during second and third ring encounters are slightly increased – most probably attributable to the system-lag and resultant phase-shift in rudder deflection.

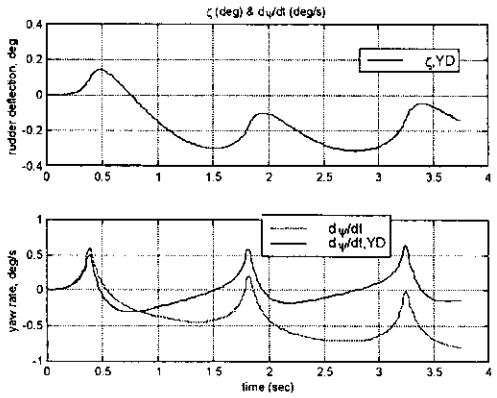

Figure 5 – YD-ON rudder deflection, and a comparison between yaw rate with zero ζ (Case (i)) and yaw rate with YD-ON ζ (Case (ii)).

The rudder deflection, driven by YD-ON is shown in Figure 5. At the selected gain of –1 and with very small time interval between vortex core passages, the developed yaw rate and subsequently developed rudder deflection ($\zeta = \int\{\partial\zeta/\partial t\}dt$) magnitudes are small, and the YD is not able to soften the yaw rate peaks associated with the yaw acceleration impulses through each vortex core.

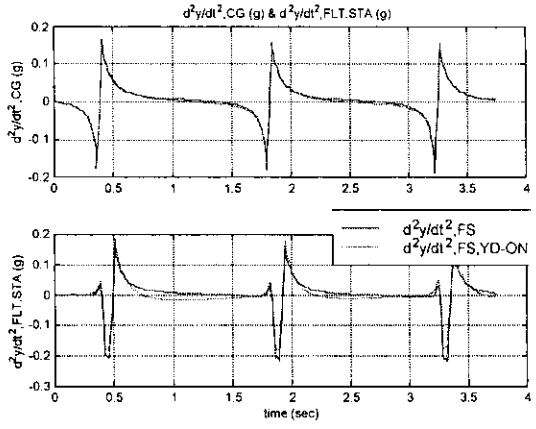

Figure 6 – Lateral acceleration at the CG and lateral acceleration at the FLT.STA (expressed as an inertial reaction acceleration, in other words a lateral acceleration to the left will result in an inertial acceleration to the right, which is selected as the positive direction for inertial reaction accelerations).

Figure 6 illustrates the calculated inertial reaction accelerations at the FLT.STA. Also reproduced is the CG lateral acceleration. Compared to the latter, the FLT.STA. inertial reaction accelerations are roughly anti-phase, principally because the dominant term is the yaw acceleration, due to the large moment arm between CG and FLT.STA. positions. The moment arm 'magnifies' the effects of yaw acceleration – neglecting lag, a -0.15 rad/sec^2 yaw acceleration equates to about +0.3 lateral g inertial reaction at the FLT.STA. Peak lateral g reaction values at the FLT.STA. are seen to vary between about 0.17g and –0.21g. The YD-ON reduces the FLT.STA. lateral 'g' reaction by about 0.03g.

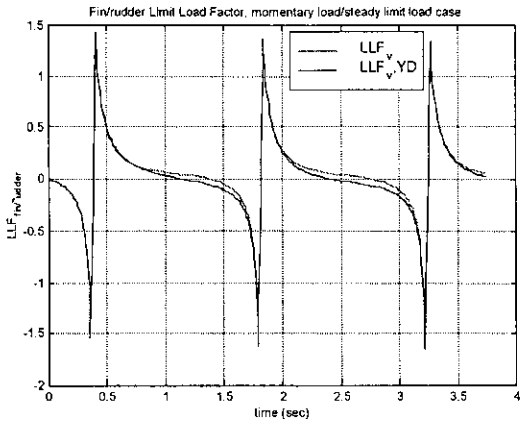

Figure 7 – Limit Load Factor for the vertical stabiliser (fin/rudder), expressed as the ratio between momentary unsteady load, as calculated, and the rationalised critical design limit load case.

For the two cases, the derived Limit Load Factor (LLF_V) curves for the vertical stabiliser (fin/rudder combination) are presented in Figure 7. The peak LLF_V magnitudes vary between about 1.3 and 1.6, a value of 1.0 equating to the magnitude of the critical manoeuvre design limit load, as rationalised earlier. Often in aeronautical structural design a factor of 1.5 is used to differentiate between limit and ultimate design loads.

The use of the LLF_V formulation emphasises the asymmetry between positive and negative (*i.e.* right and left, respectively) loading as each vortex core is traversed, partly attributable to the asymmetry of the induced-sideslip curve of Figure 3, the assumed unperturbed state at t=0, and the responsive motion to each vortex passage.

The operation of the yaw damper does not have any significant effect upon peak LLF_V magnitudes (Figure 7).

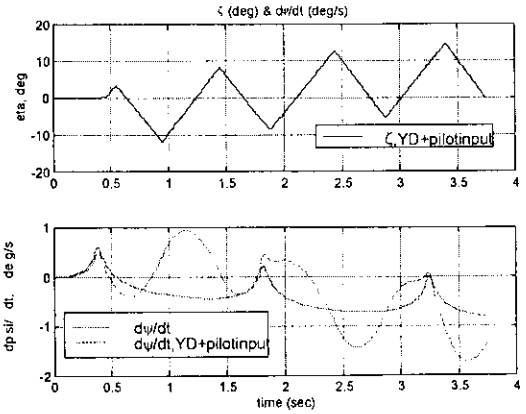

Figure 8 – Applied rudder deflection, in accordance with the HMI-system model, and resultant yaw rate (Case (i) yaw rate included for comparison).

Case (iii), Pilot-actuated rudder deflection

The pilot-actuated rudder deflection analyses (Case (iii)) have been undertaken in the same manner as the previous cases – initially the same YD-ON rigid body analysis, thereafter taking into account the lags introduced by loaded-

fuselage transverse-bending flexibility, again using the model described previously. The lateral accelerations and associated inertial reaction accelerations at the FLT.STA position have been calculated using a range of HMI-system lags from 25ms to 100ms.

The resultant Case (iii) applied rudder deflection curve for a HMI-system lag of 50ms is shown in Figure 8, together with the developed yaw rate curves (the Case (i) curve is also replicated in Figure 8). It is seen that the rudder deflection curve exhibits reversals between about $\pm 10°$ ζ. In response, the yaw rate reverses, but, principally due to the short duration of each rudder application, developed yaw rates are of low magnitude.

Resultant yaw acceleration and CG lateral acceleration (rigid body) curves are presented in Figure 9, for an HMI-system lag of 50ms. There is observed to be significant coupling between pilot-actuated rudder deflections and induced-sideslip from the right, upon approaching and penetrating each vortex core. The resultant yaw accelerations increase by 30-35%, compared to Case (i) yaw acceleration magnitudes.

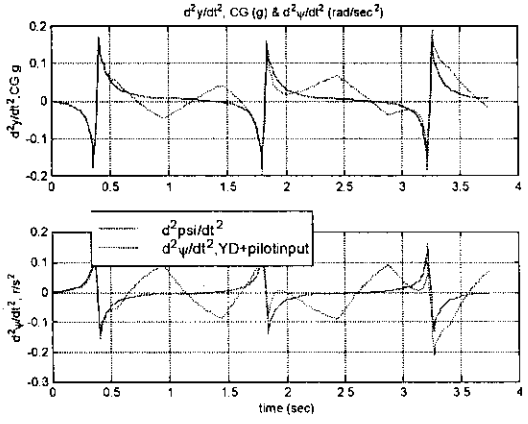

Figure 9 – Case (iii) yaw acceleration and CG lateral acceleration for 50ms HMI-system lag, Case (i) results are replicated for comparison.

The resulting inertial reaction to the lateral acceleration at the FLT.STA is presented in Figure 10 (note the change of sign, as a reaction). By the time of the third vortex ring encounter, the rudder/vortex coupling has amplified the inertial reactions by 0.1g. Encounters with subsequent vortex rings possibly might result in further increases in lateral acceleration.

The associated LLF_V peak values have been amplified by the rudder/vortex coupling (refer to Figure 11). LLF_V magnitudes of 2 have been achieved, which amount to twice the rationalised critical design limit load case.

Choice of HMI-system model and decision-making

Having observed the output for the chosen HMI-system model, it is now worthwhile to examine the decision-making, if any, that would be associated with such a model.

Because the vortex encounter environment is highly dynamic within the time domain, high gain human processing of input data and high bandwidth outputs may be appropriate – to the point where sideslip reversal rates of 200 deg/sec and resultant yaw acceleration reversal rates (Figure 9) of about 2.8 rad/sec^3 might result in reactive human control. Reactive control for the present model has been selected and is defined as the condition where human output is the result of reactive brain processing, without conscious decision-making being involved in the processing loop. Furthermore, it is assumed in this instance that reactive control results in control actuator rate saturation.

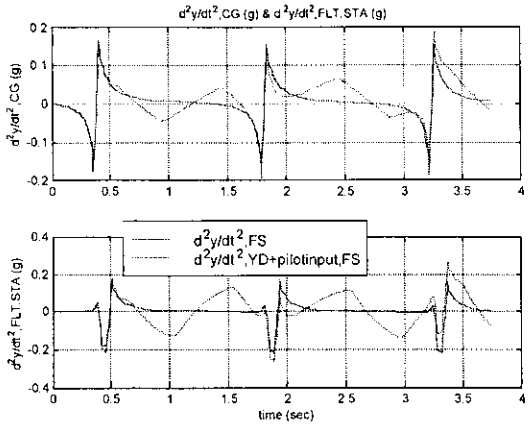

Figure 10 – Responsive lateral inertial reaction acceleration curve at the FLT.STA., Case (iii) with 50 ms lag – for comaprison, CG lateral load acceleration, Case (i) presented for both also.

Various scenarios can be considered: if a pilot, recovering from sensory g-loc whilst tactically manoeuvring, visually senses that the aircraft is flying in close proximity towards the ground, a stick-back recovery would be reactive, most probably commenced without any conscious decision being made that the actions should be undertaken. On the other hand, a pilot encountering pitch-plane homogenous turbulence of monotonically-increasing intensity, most probably would decide to do nothing initially, except monitor the sensory inputs. At some point the pilot would make a conscious decision to ameliorate the turbulence loading and provide measured control systems-inputs (as an output of conscious-loop brain processing). However, if a marked step-increase in turbulence intensity coincided with the decision to intervene, the brain processing and output might possibly become reactive – such as an immediate grab-for and retardation of the thrust levers and immediate grab-for the control column/stick and activation of the autopilot disconnect switch on the column. If the turbulence intensity was high enough, it might cause autopilot disconnect, the effect of which could possibly exacerbate turbulence-induced loads and accelerations and result in a reactive human pilot response also.

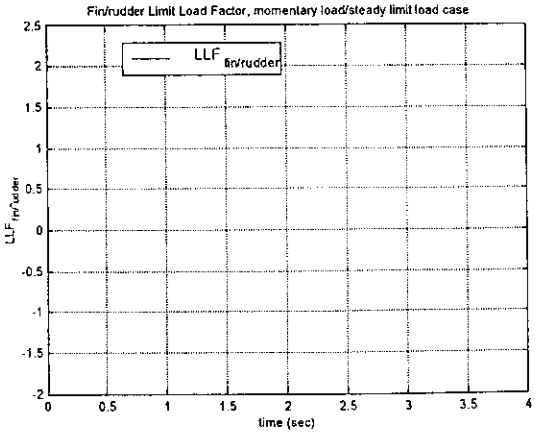

Figure 11 – Case (iii) LLF_V curve, 50ms lag.

Homogenous turbulence will also provide lateral and directional perturbations – mostly felt as sideways accelerations at the FLT.STA. A pilot, experienced on Type,

would accept some level, set by experience, of such vibratory excitation without initiating intervention. Sensorily, the excitation would be perceived by seat-cushion pressure and bodily sway. At what point would reactive intervention be initiated?

The point of reactive control initiation would require an extremely compelling sensory cue. Hence, it is reasoned that the point of reactive intervention would coincide with the occurrence of one or more sensory inputs which are overwhelmingly compelling: for example, that point at which any unrestrained item was laterally accelerated from its resting position and visually observed to slide or aurally heard to slide or fly across the flight station. Noting that resting frictional force is generally about 0.3g, any lateral acceleration or acceleration reversal above this value would overcome resting frictional force and accelerate any and all objects. Suddenly seeing and/or hearing any object move sideways across the cockpit with an instant flurry would likely be the 'GO' trigger to commence reactive control inputs, a commencement which would be unlikely to involve conscious decision-making. Indicators of a lack of conscious decision-making would be the control input rates and a lack of any remark from the pilot regarding intended actions.

Such a rationale underpins the selection, in the present engineering study, of a 0.3g acceleration or acceleration increment as the threshold for the 'GO' trigger that initiates HMI-system reactive control.

As a test for this hypothesis, given that vertical-axis vortex core encounters (whether vortex rings or line vortices) can be expected to be very rare events (to the extent that most pilots would not have experienced one such event, let alone several events), the reactive sense of control inputs should be examined. If a pilot feels a positive g inertial reaction acceleration (seat pressure downwards), the reactive control input is stick/column-forward to unload – the correct reaction; *vice versa*, upon feeling a negative g inertial reaction acceleration (seatbelt strap pressure upwards), the reactive control input is stick/column-back to load – again the correct response. In both cases the reactive control inputs are in the direction of driving the aircraft towards the inertial reaction acceleration (*i.e.* to position the aircraft acceleration vector to be parallel to the inertial reaction acceleration vector).

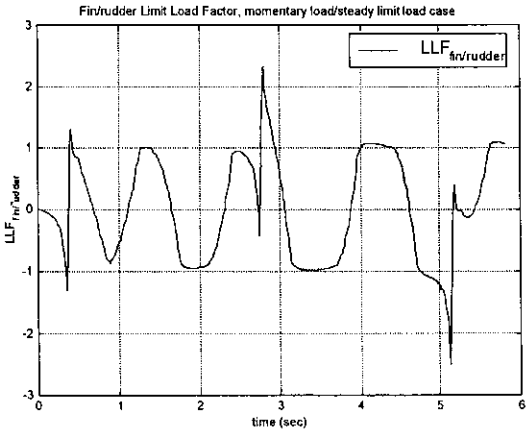

Figure 12 – Fin/rudder limit load factor, for the study case of a Δx=5a vortex ring separation distance

In accordance with this 'law', a pilot sensing a lateral inertial reaction acceleration to the left say, above the 'GO' trigger threshold, would result in a reactive control input to accelerate the aircraft to the left also – left rudder, the correct input direction, but the phase-lag of which could result in loads coupling with subsequent unsteady flow angles and dynamic pressures attributable to coherent flow structures in the freestream air.

Variation of vortex ring separation, Δx

A simulated HMI interaction has also been studied for a vortex ring separation of Δx = 5a ('a' being the vortex ring radius), to investigate the effect upon the interaction of a variation of vortex ring spacing. The results are shown in Figures 12 and 13. Compared to the 3a vortex ring separation, for the larger 5a separation, the model predicts 25% greater fin/rudder peak limit load factors (2.5, observed in Figure 12, compared with 2).

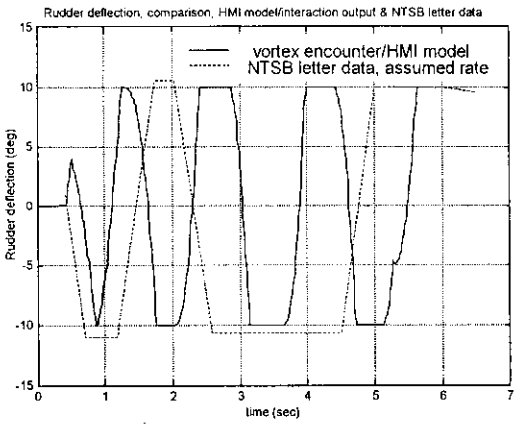

Figure 13 – HMI model rudder deflection output, Δx=5a vortex ring separation distance, wake encounter accident rudder deflection peak behaviour from Ref. 16, at an unknown but assumed movement rate of 39 deg/sec.

Figure 13 shows the applied rudder deflection, as an output of the interaction model. In Figure 13 is included the transcribed rudder deflection behaviour (from the verbal description footnoted in Ref.16, which states that *'within about 7 seconds, the rudder travelled 11° right for 0.5 second, 10.5° left for 0.3 second, between 11° and 10.5° right for about 2 seconds, 10° left for about 1 second, and, finally, 9.5° right before the data became unreliable'*) obtained from preliminary analysis of flight data recorder (FDR) data during and following a turbulence encounter consistent with a wake vortex encounter (wake state unknown) experienced by a jet transport aeroplane[16]. Structural failure during the accident sequence included failure of the fin to fuselage attachments and separation of the fin and rudder from the fuselage[16]. Recorded rudder pedal movements corresponded with rudder movements[16]. The accident is still under investigation. Potential causes of the rudder movement under examination include rudder system malfunction as well as flight crew action, as cited in Ref. 16.

The movement rate for the rudder is unknown. In the data plot of Figure 13 a rate of 39 deg/sec has been assumed. From the verbal description of Ref.16, the preliminary analysis indicated that the rudder dwelled at left and right peak deflections for about 4 seconds, leaving a travelling time of about 3 seconds. If the peak rudder deflections are summed, they amount to about 94° of movement, which in the available travelling time would amount to an average movement rate of about 31.3 deg/sec. As an average rate and if attributable to human pilot-input, this would represent high gain inputs, some of which would be likely to have been system-rate saturation inputs. This would be evidence of reactive human control, which has been used in the HMI

model of the present study. Possibly, vertical-plane vortex rings might need to be considered as coherent flow structures within the encountered wake vortices to which Ref.16 refers.

CONCLUSIONS

An engineering study has been conducted into the unsteady airloads and acceleration effects of a Crow instability vortex wake encounter by a widebody-type jet transport aircraft, specifically for the hypothesised case where the vortex rings of the Crow instability have rotated to the vertical position and the aircraft penetrates the vortex ring cores.

For this hypothesised vortex ring configuration, the encounters consist of directionally reversing perturbations of sideslip magnitude $\pm\beta$=10°, which are analysed to produce momentary loads which are in exceedance of the critical design manoeuvring load case.

For a reactive control HMI model, with FLT.STA lateral acceleration threshold as the ON-OFF-ON switch logic, and a 'global' allowance for fuselage transverse flexibility (*albeit* with no amplitude magnification), it is demonstrated that, pilot rudder inputs could couple with vortex-induced sideslip perturbations and increase the acceleration / fin loads peak magnitudes by 30-35%. With a full allowance for vibratory modal excitation, super-circulation induced by vortex-shearing and convection, further HMI model refinements, it is possible that the coupling magnitude could be greater still.

The study indicates that inflight probing of aircraft wakes is desirable, in order to survey the detailed nature of the Crow instability mechanism of trailing vortex wakes and, in particular, to test the hypothesis of vortex ring rotation to the upright position.

REFERENCES

[1] Aeronautical Information Publication (A.I.P.) Canada, Rules of the Air and Air Traffic Services, RAC 4.1.1, Wake Turbulence. Transport Canada.

[2] Rossow, V.J. and James, K.D., "Overview of Wake-Vortex Hazards During Cruise," *Journal of Aircraft*, Vol. 37, No. 6, 2000, pp. 960-975.

[3] Crow, S.C., "Stability Theory for a Pair of Trailing Vortices," *AIAA Journal*, Vol. 8, No. 12, 1970, pp. 2172-2179.

[4] Mather, G. K., "A Note on Some Measurements made in Vortex wakes behind a DC8," *Laboratory Memorandum No. FR-48, National Aeronautical Establishment*, Ottawa, 1967.

[5] Treddenick, D. S., "Flight Measurements of the Vortex Wake behind a Convair 880", *Report No. LTR-FR-4, National Aeronautical Establishment*, Ottawa, 1968.

[6] Brown, A. P., "Line vortex modelling of free vortices encountered during low-level flight operations over the Boreal Forest", AIAA Atmospheric Flight Mechanics Conference, 2002.

[7] MacPherson, J. I. And Betts, A. K., "Aircraft encounters with strong coherent vortices over the boreal forest," *Journal of Geophysical Research*, Vol. 102, No. D24, Pages 29,231-29,234, December 26, 1997.

[8] Batchelor, G.K., "An Introduction to Fluid Mechanics", Cambridge University Press, 1974.

[9] Jones, R. T., "The Unsteady Lift of a Wing of Finite Aspect Ratio," *NACA Report 681*, 1940.

[9] Fung, Y. C., "An Introduction to the Theory of Aeroelasticity," *Dover Publications*, 1969.

[10] Lomax, T. L., "Structural Loads Analysis for Commercial Transport Aircraft: Theory and Practice", *AIAA Education* Series, 1996.

[11] Nelson, R.C., "Flight Stability and Automatic Control", McGraw Hill International Editions, Aerospace Series, 1989.

[12] Federal Aviation Administration, "Part 25 – Airworthiness Standards: Transport Category Airplanes," CFR 14, Aeronautics and Space.

[13] Joint Aviation Authorities, "Part 25 – Airworthiness Standards: Transport Category Airplanes," JAR 25.

[14] Hussey, M., "Fundamentals of Mechanical Vibrations", Macmillan Publishing Company, 1983.

[15] Abramson, N., "An Introduction to the Dynamics of Airplanes," Dover Publications, 1958.

[16] Safety Recommendation, American Airlines flight 587. National Transportation Safety Board, A-02-01 and –02, February 8, 2002.

12